ISSN 1 746-7233, England, UK
World Journal of Modelling and Simulation
Vol. 11 (2015) No. 2, pp. 145-160

Modeling and simulation of dispersed two-phase flows of bubbles, drops and particles*

Madhukant Sharma[1], B.V.Rathish Kumar[2†], Vivek Sangwan[3], S.K.Murthy[4]

[1] Indian Institute of Technology Madras, Chennai - 600036 India
[2] Indian Institute of Technology Kanpur, Kanpur - 208016, India
[3] Defence Institute of Advance Technology, Pune - 411025, India
[4] Thapar Unviersity, Patiala - 147004, India

(*Received September 22 2014, Accepted April 11 2015*)

Abstract. An averaged two-fluid flow model for dispersed two-phase flows of Bubbles, Drops and Particles based on similarity criteria and mixture viscosity concept has been analyzed. Ordinary differential equations describing the relative velocities of liquid and gas phases together with the ordinary differential equation for the density of gas phase are considered as Initial Value Problems (IVPs). The approximate solutions of IVPs have been investigated by different numerical schemes to identify a reasonably efficient numerical scheme for future practical considerations. Further, based on modified Ishii et al.[8] model the effect of variation of void fraction and phase velocities of the fluids across the cross section of the pipe have been investigated. The equations of Kumar et al.[11] are used to calculate the Bubble size at the mixer orifice exit. Void fraction and slip at different locations are determined for a model of nitrogen - mercury system set up, where the mass fluxes varying from 0.125 to $2.302\ kg/sm^2$ for nitrogen and 5.52×10^3 to $12.26 \times 10^3\ kg/sm^2$ for mercury. Finally, the predicted values have been compared with the experimental data. Also, influence of pressure and mass flow rates on gas and liquid velocities, void fraction, density of gas, friction and drag coefficients have been investigated at the end.

Keywords: modeling and simulation, two-phase flow, bubbly flow, runge-kutta method

1 Introduction

Studies related to ADS (Accelerator Driven Sub-critical reactor Systems) Nuclear Reactors have been taken up in view of their extremely high level of inherent safety and the ability to utilize thorium and to transmute nuclear waste generated in nuclear power reactors. These ADS systems contain two - phase vertical flows consisting of high density liquid metals and suitable gas-vapor. Optimum design of ADS requires accurate modeling of two-phase flows in the riser. The Schematic of the loop is shown in Fig. 2 which has been taken from Satyamurthy et al.[15]. The loop consists of spallation simulation region, riser (annular cross-section of proton beam pipe and riser pipe) where liquid metal flows upwards after collecting the heat deposited in the window by the low energy beam/plasma heat source. Suitable gas is injected in the Mixer which is located at the bottom of raiser. Due to this, two-phase flow is created in the riser pipe, thus reducing the average density of the flow, and hence creating a large pressure head in the loop and providing the required pressure head. From the exit of the riser the liquid metal flows in to a separator. The two-phases are separated in the Separator by gravity. The liquid metal flows down in the downcomer, which also acts as heat exchanger (double pipe heat - exchanger cooled by air/nitrogen). From the bottom of the downcomer, flow turns around and enters

* This work has been carried out under the project (2008/34/15-BRNS/4008)funded by BARC, Mumbai. Third and fourth authors are thankful to BARC for providing them the research assistance while carrying out this project work.
† Corresponding author. *E-mail address*: bvrk@iitk.ac.in

into the nozzle and from there enters into the riser (annular cross-section). Nitrogen gas, which is separated in the separator, is re-circulated either using a compressor or let out to ambient. So, mixer is one of the key components of gas-driven target loop. Nitrogen/Argon gas is injected into LBE (Lead-Bismuth-Eutectic) in the Mixer through a distributor having large number of small holes (1 mm diameter)[15]. Number of holes, their distribution and gas velocity in the holes decide effective coupling of liquid and gas. Ideally we require large number of small bubbles distributed uniformly in the LBE across the pipe cross-section leading to minimum slip and providing bubble flow regime. However, in real system, due to limitation of distributor and lower limit on the gas velocity, it is not possible to have ideal mixer configuration. Therefore, one has to carry out detailed two-phase flow analysis to study the performance of actual mixer and to arrive at optimum configuration.

A general transient two-phase flow problem can be formulated either by a two-fluid model or mixture model. In the two-fluid model each phase considered separately, hence the model is formulated in terms of two sets of conservation equations. A mixture model (i.e., for an example Drift-Flux model) can be obtained by replacing the two-momentum equations by a mixture momentum equation and a relative velocity correlation. Therefore, for mixture model formulation, a relative velocity correlation is required whereas for two-fluid model formulation an interfacial drag correlation should be specified. Even though the diffusion model is simple, compared to the two-fluid model, but many important features of two-phase flow are lost (e.g., initial conditions of the mixer cannot be incorporated in the flow, void fraction cannot be determined explicitly from the equations etc.). However, the actual flow evolves from multi-bubble to churn-turbulent to slug flow along the riser.

The recent developments in multi-phase two-fluid model and solvers can be found in literature. Guo et al.[5] employed difference method to investigate the analytic results concerning the existence and uniqueness of global strong solutions for a one dimensional viscous two-phase flow model when both the initial liquid and gas masses connect to vacuum discontinuously. While Jannike et al.[16] studied a one dimensional two fluid model numerically and applied the results to simulate gas-solid cold-flows in fluidised beds. The simulation results are compared to results of a two-dimensional model. Recently, Prasanna et al.[13] designed a numerical scheme which is implemented to simulate one dimensional multi-phase flow based on drift flux model in an isothermal setup with phase dissolution. For more results in this direction, we refer to [3, 6, 19] and the references therein.

It is to be noted that the ability to predict the interfacial drag or the relative velocity between phases is of considerable importance for analyzing a dispersed two-phase system under steady-state or transient conditions. For example, the designs and performances of fluidization, sedimentation, and extraction system as well as various heat transfer system can be significantly affected by a reliable interfacial drag correlation. These facts incite us to develop an averaged two-fluid model based on the work of Ishii[8], Ishii and Zuber[10] and Ishii and Mishima[9]. To be more precise, the purpose of this model is to develop constitutive relations for the drag force and the relative velocity for bubbly, droplet and particulate flows by a unified method. For doing this, we consider the drag similarity law in unified form by taking into account the effect of both motion and the presence of other particles. Also, interfacial drag force corresponding to multi-bubble, churn-turbulent and slug flow based on Ishii et al.[10] and Taitel[17] classification has been used. Moreover, simple drag similarity criteria and mixture viscosity concepts are introduced in the analysis to model an averaged two-fluid model. As a result, this unified and consistent model presents drag and relative velocity correlations which cover all concentration ranges and wide Reynolds number ranges, from the Stokes regime up to the Newton's regime, or the Churn-Turbulent Flow regime. This unified and consistent model can be useful for predicting void fractions, interfacial area, particle residence time and occurrences of flooding of concentration shock waves. As an application, we implement this averaged model to determine void fraction, interfacial drag, relative velocities of gas and liquid phases along the riser for nitrogen-mercury two-phase upward vertical flows.

This paper is organized under seven sections. Section 1 introduces the background of the problem and its importance together with remarks on the current status and motivation for the current study. In section 2 deals with the mathematical description of the proposed problem. Numerical solution methodology for the mathematical model is presented in section 3. Results obtained from the numerical simulations are discussed in section 4. Here we consider the ordinary differential equations describing the relative velocities for the liquid and gas phase together with the ordinary differential equation for the density of gas phase as Initial

value problems and simulate their approximate solutions via several numerical schemes to identify efficient scheme for future considerations. Further, we investigate the influence of pressure and mass flow rates on gas and liquid velocities, void fraction, density of gas, friction and drag co-efficient in the results and discussion section. Finally, we compare the predicted values of void fraction with the experimental data for nitrogen - mercury experimental set up. Section 5 presents the conclusions.

2 Mathematical model

In the past, different empirical or semi-empirical correlations had been obtained for solid and fluid particle systems at different Reynolds numbers and particle sizes. Existing correlations are either purely empirical formulas or they are based on analytical modelling with very limited applicable ranges, in terms of the nature of the particles and the particle Reynolds number. A number of correlations for the relative velocity could be found in the literature. However, most of them are developed from a limited number of experimental data and therefore are applicable only to a certain type of dispersed flows. And therefore the scope of our model is to look at constitutive relations for drag force and the relative velocity correlation for bubbly, droplet and particulate flows by unified method. The present analysis considers the drag similarity law in unified form, by taking into account the effect of both motion and the presence of other particles. Model is formulated in one dimensional case under certain assumptions and conditions which are as follows:

(1) The present relative velocity correlation and the formula for the drag co-efficient for multi-particle systems have been developed from the steady -state and adiabatic formulation.
(2) The additional interfacial forces due to the inertia effect and development of boundary layer in a transient flow are considered separately.
(3) The effects of heat transfer and phase changes are considered as secondary here.
(4) It is assumed that both the averaged pressure and stress in the bulk fluid and at the interface are approximately same, the three dimensional k-phase momentum equation[10] is given by:

$$\alpha_k\rho_k\left(\frac{\partial v_k}{\partial t}+v_k\cdot\nabla v_k\right)=-\alpha_k\nabla p_k+\alpha_k\nabla\cdot(\bar{\bar{\tau}}_k+\bar{\bar{\tau}}_k^T)+\alpha_k\rho_k g+M_{ik}+(v_{ki}-v_k)\Gamma_k. \tag{1}$$

The conservation of the mixture momentum requires:

$$\Sigma_k M_{ik}=0, \tag{2}$$

which is the modified form of the averaged momentum jump condition.
(5) We are neglecting the lift force due to rotations of particles and the diffusion force because of the concentration gradient. Then, the generalized drag force for the dispersed phase may be modeled by a simple form [20] as:

$$M_{id}=\frac{\alpha_d F_D}{B_d}-\frac{\rho_c\alpha_d}{2}\left(\frac{1+2\alpha_d}{1-\alpha_d}\right)\frac{d}{dt}(v_d-v_c)+\frac{9\alpha_d}{2r_d}\sqrt{\frac{\mu_m\rho_c}{\pi}}\int^t\frac{d}{d\xi}(v_c-v_d)\frac{d\xi}{\sqrt{t-\xi}}. \tag{3}$$

(6) Wall is assumed to be absent here and motion is under steady state condition without phase change which reduces the multi-particle system in an infinite medium to a gravity dominated one-dimensional flow without transient effects. Then, the axial component of the momentum Eq. (1) for k-phase can be written as

$$0=-\alpha_k\frac{dp_m}{dx}-\alpha_k\rho_k g+M_{ik}. \tag{4}$$

(7) We also assumed that the surface tension effect on the pressures can be neglected. By adding the phase momentum equations and using Eq. (2), we obtain

$$\frac{dp_m}{dx}=-\rho_m g. \tag{5}$$

The drag force acting on the particle under steady - state condition can be given in terms of the drag coefficient C_D based on the relative velocity as

$$F_D = -\frac{1}{2} C_D v_r \rho_c |v_r| A_d. \tag{6}$$

Then, F_D is related to the interfacial force by

$$F_D = \frac{M_{id} B_d}{\alpha_d}. \tag{7}$$

Now, from Eqs. (4) - (7), we obtain

$$v_r |v_r| = \frac{8 g r_d (\rho_c - \rho_d)(1 - \alpha_d)}{3 C_D \rho_c}, \tag{8}$$

where the mean radius of the particle is defined by

$$r_d = \frac{3 B_d}{4 A_d}. \tag{9}$$

On the other hand, for a system with a single particle in an infinite medium, the force balance is given by equation

$$r_d^o = \frac{3}{8} (v_{r\infty}^o)^2 C_{D\infty}. \tag{10}$$

Moreover, in a dimensional form, the force balance equation is

$$v_{r\infty} |v_{r\infty}| = \frac{8 g r_d (\rho_c - \rho_d)}{3 C_{D\infty} \rho_c}. \tag{11}$$

In general, the drag law for a single particle can be expressed by $C_{D\infty} = C_{D\infty}(N_{Re\infty})$, where the Reynolds Number $N_{Re\infty}$ is given by

$$N_{Re\infty} = \frac{2 r_d \rho_c |v_{r\infty}|}{\mu_c}. \tag{12}$$

By comparing a single particle system to a multi - particle system, we get from Eqs. (8) and (11)

$$C_{D\infty}(N_{Re\infty}) = \frac{C_D(N_{Re})}{(1 - \alpha_d)} \left(\frac{v_r}{v_{r\infty}} \right)^2. \tag{13}$$

Here the Reynolds Number is given by

$$N_{Re} = \frac{2 r_d \rho_c}{\mu_m} |v_r|. \tag{14}$$

By knowing the mixture viscosity and the dependence of C_D on N_{Re}, Eq. (13) can be solved for the velocity ratio $\frac{v_r}{v_{r\infty}}$ to obtain the relative velocity in terms of the single - particle terminal velocity. In the present analysis, we extend the linear correlation[18] for the mixture viscosity for fluid particles along the power relation[14] for solid particles based on the maximum packing α_{dm}. Thus, we have [7]

$$\frac{\mu_m}{\mu_c} = \left(1 - \frac{\alpha_d}{\alpha_{dm}} \right)^{-2.5 \frac{\alpha_{dm}(\mu_d + 0.4\mu_c)}{\mu_d + \mu_c}}. \tag{15}$$

The maximum packing α_{dm} for solid particle systems ranges from 0.5 to 0.74. However, $\alpha_{dm} = 0.62$ suffices for most of the practical cases. For a bubbly flow, theoretical α_{dm} can be much higher because of the deformation of bubbles. In the absence of turbulent motions and particle coalescence, the void fraction in a fluid particle system can be as high as 0.95. By taking maximum packing α_{dm} to be unity, it is possible to include these foam or dense packing regimes in the analysis. Therefore, for fluid particle systems, we take $\alpha_{dm} = 1.0$.

The following conservation and other auxiliary equations have been used.

2.1 Combined two-phase momentum equation

Under the assumptions and conditions stated above, and area averaging Eq. (1) , the following one dimensional momentum equations for gas and liquid phase can be obtained:

$$\frac{d}{dx}(C_{vg}\alpha\rho_g u_g^2) = -\alpha\frac{dp}{dx} + \frac{d}{dx}\left\{\alpha\left(\bar{\bar{\tau}}_{gxx} + \bar{\bar{\tau}}^T_{gxx}\right)\right\} - \frac{4\alpha_{gw}\bar{\bar{\tau}}_{gw}}{D} - \alpha\rho_g g + M_g^d, \tag{16}$$

$$\frac{d}{dx}(C_{vl}(1-\alpha)\rho_l u_l^2) = -(1-\alpha)\frac{dp}{dx} + \frac{d}{dx}\left\{(1-\alpha)\left(\bar{\bar{\tau}}_{lxx} + \bar{\bar{\tau}}^T_{lxx}\right)\right\} - \frac{4(1-\alpha_{lw})\bar{\bar{\tau}}_{lw}}{D} - (1-\alpha)\rho_l g + M_l^d, \tag{17}$$

where C_{vk}, α_{kw}, M_k^d, and τ_{kw} are the distribution parameter of momentum flux, wall void fraction, total interfacial shear force and wall shear stress for k-phase respectively. We invoke the following considerations:

(1) $\frac{4}{D}\{\alpha_{gw}\bar{\bar{\tau}}_{gw} + (1-\alpha_{lw})\bar{\bar{\tau}}_{lw}\}$ term is the frictional pressure drop at the walls. And this is expressed as

$$f_R = \varphi_{lo}^2\left(\frac{dp}{dx}\right)_{fr_{lo}}. \tag{18}$$

(2) Since, the stress distribution in the fluid and in the dispersed phase should be similar and the values of $\left(\alpha\left(\bar{\bar{\tau}}_{gxx} + \bar{\bar{\tau}}^T_{gxx}\right)\right)$ and $\left((1-\alpha)\left(\bar{\bar{\tau}}_{lxx} + \bar{\bar{\tau}}^T_{lxx}\right)\right)$ are generally small[7], therefore, the effect of the shear gradient on the mean local velocity can be neglected. Hence, we are neglecting the term $\frac{d}{dx}\left\{\alpha\left(\bar{\bar{\tau}}_{gxx} + \bar{\bar{\tau}}^T_{gxx}\right) + (1-\alpha)\left(\bar{\bar{\tau}}_{lxx} + \bar{\bar{\tau}}^T_{lxx}\right)\right\}$.

(3) C_{vg} and C_{vl} are related to void fraction, velocity profile, shape and for our liquid metal system. Hence, for all practical purposes both C_{vg} and C_{vl} may be approximated by numerical value 1.0.

On combining Eqs. (16) and (17) along with the considerations (i), (ii), (iii) and the assumption (2), we get the following combined momentum equation

$$\alpha\rho_g u_g\frac{du_g}{dx} + (1-\alpha)\rho_l u_l\frac{du_l}{dx} = -\frac{dp}{dx} - \{\alpha\rho_g + (1-\alpha)\rho_l\}g - \varphi_{lo}^2\left(\frac{dp}{dx}\right)_{fr_{lo}}. \tag{19}$$

The frictional pressure drop assuming the flow to have liquid metal properties has been determined as follows:

$$\left(\frac{dp}{dx}\right)_{fr_{lo}} = \frac{8f_{lo}(m_l+m_g)^2}{D^5\pi^2\rho_l}. \tag{20}$$

Also, the two - phase correlation term φ_{lo}^2 is determined based on Friedel correlation[2] as follows:

$$\varphi_{lo}^2 = (1-Q)^2 + Q^2\frac{\rho_l f_{go}}{\rho_g f_{lo}} + \left[\frac{3.24Q^{0.78}(1-Q)^{0.24}\left(\frac{\rho_l}{\rho_g}\right)^{0.91}\left(\frac{\mu_g}{\mu_l}\right)^{0.19}\left(1-\frac{\mu_g}{\mu_l}\right)^{0.7}}{F_r^{0.045}W_e^{0.035}}\right], \tag{21}$$

where, $F_r = \frac{G^2}{gD\rho_t^2}$, $W_e = \frac{G^2D}{\rho_t\sigma_l}$, ρ_t (two-phase density) $= \frac{\rho_l\rho_g}{Q\rho_l+(1-Q)\rho_g}$ and $G = \frac{(m_l+m_g)}{A}$. And f_{lo} is determined based on Colebrook equation[4]) as follows:

$$\frac{1}{\sqrt{f_{lo}}} = -2log\left(\frac{\epsilon}{3.7D} + \frac{2.51}{N'_{Re}\sqrt{f_{lo}}}\right). \tag{22}$$

Similar equation is used for the f_{go}.

2.2 Liquid metal and gas continuity equations

Since liquid is incompressible, ρ_l will be scalar quantity whereas ρ_g may or may not be scalar quantity. Indeed, we assumed that ρ_g is a function of x. Also, $u_l,\ u_g$ & α are the functions of x only. (Since we are in one dimensional case only).

$$\rho_l u_l (1-\alpha) A = m_l, \tag{23}$$

$$\rho_g u_g \alpha A = m_g. \tag{24}$$

On differentiating (23) and (24) w.r.to x and eliminating $\frac{d\alpha}{dx}$, we have

$$\frac{d\rho_g}{dx} = -\frac{\rho_g}{u_g}\frac{du_g}{dx} - \frac{(1-\alpha)\rho_g}{\alpha u_l}. \tag{25}$$

2.3 Momentum equation of the bubble

To get the momentum equation of the bubble, we are making the following assumptions:

(1) We are neglecting the viscous and turbulent stress. Also, wall shear stress term in the gas momentum equation has been neglected due to low void fraction near the wall[19].
(2) We are neglecting the effect of interfacial shear and the void gradient as they are important in annular flows[9].
(3) Basset force is neglected in our model.

Then the momentum equation of the bubble is given by

$$\rho_g u_g \frac{du_g}{dx} = -\frac{dp}{dx} - \rho_g g - \frac{F_D}{V_b} - \frac{F_{vm}}{V_b}. \tag{26}$$

2.4 Equation of state of gas

$$p = \rho_g RT = C_1 \rho_g. \tag{27}$$

where R is the gas constant and the temperature of gas/liquid, T, is assumed to be constant. And from (27), we have

$$\frac{dp}{dx} = C_1 \frac{d\rho_g}{dx}. \tag{28}$$

2.5 Effect of cross-sectional variation

Ishii and Mishima[9] have proposed that under the following conditions, the pipe diameter should be considered small.

$$\alpha < \frac{1}{C_0} \text{ and } j_g \sqrt{\frac{\rho_g}{(\rho_l - \rho_g) g D}} > \alpha - 0.1$$

where j_g is averaged gas volumetric flux, α is the averaged void fraction for gas phase and C_0 is given by

$$C_0 \cong 1.2 - 0.2\sqrt{\frac{\rho_g}{\rho_l}}. \tag{29}$$

When the above conditions are satisfied, the cross-sectional variation of α and phase velocities should be taken into consideration by modifying the relative velocities of the phases as follows:

$$(u_g - u_l) \models \left(\frac{1 - C_0\alpha}{1-\alpha}\right)(u_g - C_0 u_l). \tag{30}$$

2.6 Virtual mass force

Virtual mass force F_{vm} incorporated in the momentum equation for gas phase has been taken from the following equations developed for bubbly flow by Ishii[9]:

$$\frac{F_{vm}}{V_b} = C_{vm}\rho_l \left[\frac{D_d}{Dt} < v_r > - < v_r > \nabla v_c\right]. \tag{31}$$

where $< v_r >$ is area averaged relative velocity and

$$C_{vm} = 0.5\left(\frac{1+2.0\alpha}{1-\alpha}\right),$$
$$< v_r >= (u_g - u_l) \models \left(\frac{1.0 - C_0\alpha}{1.0-\alpha}\right)(u_g - C_0 u_l).$$

Since, the motion is steady state, therefore, on expanding and averaging the above equation, we get

$$\frac{F_{vm}}{V_b} = C_{vm}\rho_l \left(\frac{1.0-C_0\alpha}{1.0-\alpha}\right)\left[u_g\left(\frac{du_g}{dx}\right) + (C_0 u_l - (1+C_0)u_g)\left(\frac{du_l}{dx}\right)\right]. \tag{32}$$

From Eqs. (19), (25), (26), (28) and (32), we obtain the following set of ordinary differential equations in terms of u_g and u_l:

$$\frac{du_g}{dx} = \frac{N_r}{D_r}, \tag{33}$$

$$\frac{du_l}{dx} = \frac{\left\{S_1 - \left(\rho_g\alpha u_g - \frac{C_1\rho_g}{u_g}\right)\frac{du_g}{dx}\right\}}{(1-\alpha)\rho_l u_l - \frac{C_1(1-\alpha)\rho_g}{\alpha u_l}}, \tag{34}$$

where

$$\begin{aligned}
N_r &= S_1\left[\rho_l C_{VM}\left(\frac{1-C_0\alpha}{1-\alpha}\right)\{C_0 u_l - (C_0+1.0)u_g\} - \frac{C_1(1-\alpha)\rho_g}{\alpha u_l}\right] \\
&\quad + \left(\rho_g g + \frac{F_D}{V_b}\right)\left[(1-\alpha)\rho_l u_l - \frac{C_1(1-\alpha)\rho_g}{\alpha u_l}\right], \\
D_r &= \left(\alpha\rho_g u_g - \frac{C_1\rho_g}{u_g}\right)\left[\rho_l C_{VM}\left(\frac{1-C_0\alpha}{1-\alpha}\right)\{C_0 u_l - (C_0+1.0)u_g\} - \frac{C_1(1-\alpha)\rho_g}{\alpha u_l}\right] \\
&\quad - \left[\rho_g u_g - \frac{C_1\rho_g}{u_g} + C_{VM}\rho_l u_g\left(\frac{1-C_0\alpha}{1-\alpha}\right)\right], \\
S_1 &= -\{\alpha\rho_g + (1-\alpha)\rho_l\}g - \varphi_{lo}^2\left(\frac{dp}{dx}\right)_{fr_{lo}}.
\end{aligned} \tag{35}$$

Now, we put (33), (34) and (25) as an initial value problem. Classification of the flow structure is determined based on Taitel et al.[17] as follows. For void fraction α less than 0.25, the flow is assumed to be in the multi-bubble regime. Beyond that, the flow is churn-turbulent of slug depending upon whether x is less than the entrance length 'I_E' or not. The interfacial drag force is determined based on Ishii and Mishima[9] work. For the multi-bubble regime, the drag force is determined as follow

$$F_D = 0.5\rho_l V_b\sqrt{\frac{g(\rho_l-\rho_g)}{\sigma_l}}\left[\frac{1+17.67(1-\alpha)^{\frac{9}{7}}}{18.67(1-\alpha)^{1.5}}\right]^2 (u_g-u_l)|(u_g-u_l)|. \tag{36}$$

When α is greater than 0.25 and x is less than entrance length 'I_E' , then flow is churn - turbulent and the drag force is given by

$$F_D = \left(\frac{4}{3}\right)\rho_l A_d(1-\alpha)^2(u_g-u_l)|(u_g-u_l)|. \tag{37}$$

The entrance length I_E is defined as:

$$\frac{I_E}{D} = 40.6\left[\frac{(\alpha u_g - (1-\alpha)u_l)}{\sqrt{gD}} + 0.22\right]. \tag{38}$$

And for the slug flow, the drag force is given by

$$F_D = 4.9\rho_l A_d(1-\alpha)^3(u_g - u_l)|(u_g - u_l)|. \tag{39}$$

3 Numerical schemes

Several analytical techniques exist for finding the solutions of differential equations. It is a fact that a mathematical model for a physical system, owing to the nonlinearity either in the geometry or in the governing equations, cannot be solved analytically many times. In such cases, the numerical techniques are useful. In numerical methods instead of finding a relation between dependent and independent variable, we find the approximate numerical values of the dependent variables for certain values of the independent variables. In the present paper, we are solving our problem by RungeKutta method of order 2, 4, 6 and also by MilneSimpsons method which is a Predictor Corrector method. A brief description on RungeKutta methods and MilneSimpsons method is as follows:

3.1 Runge-Kutta (RK) methods:

For solving the IVP $\frac{dy}{dx} = f(x,y)$ with $y(x_0) = y_0$ to get $y_1 = y(x_1)$ where $x_1 = x_0 + h$, x_0 is the initial point and h is step size. Runge-Kutta Method of order four is given by

$$y_1 = y_0 + \frac{h}{6}(K_1 + 2K_2 + 2K_3 + K_4),$$
$$K_1 = f(x_0, y_0),\ K_2 = f\left(x_0 + \frac{h}{2}, y_0 + \frac{K_1}{2}\right),\ K_3 = f\left(x_0 + \frac{h}{2}, y_0 + \frac{K_2}{2}\right),\ K_4 = f(x_0 + h, y_0 + K_3).$$

The 2nd order Runge-Kutta method is nothing but Euler's Method. We have also used an explicit sixth order Runge-Kutta Method which is given by Luther[12].

3.2 Milne-Simpson's predictor-corrector method (MSPCM)

The Milne-Simpson's method is not self starting method. Three additional starting values y_1, y_2 and y_3 must be given or they are usually computed by using the Runge-Kutta Method. Milne-Simpson's Predictor formula is given by:

$$y_4 = y_0 + \frac{4h}{3}(2f_1 - f_2 + 2f_3),$$
$$f_1 = f(x_1, y_1),\ f_2 = f(x_2, y_2),\ f_3 = f(x_3, y_3).$$

Then we compute $f_4 = f(x_4, y_4)$. And then, Milne's Corrector formula is: $y_4^{(1)} = y_2 + \frac{h}{3}(f_2 + 4f_3 + f_4)$. MSPCM method is derived by using Newton's formula for forward interpolation.

3.3 Algorithm for numerical solution

The governing equations are simplified algebraically and the modified non-linear Eqs. (25), (26) and (27) together with initial conditions are solved by either 2nd or 4th or 6th order RK method or by MSPCM. Basic steps involved in the computation are as follows:

(1) Choosing a step size to start the loop.
(2) Calculate the frictional pressure drop, slip, Virtual mass force and standard drag force (F_D) in different regimes in this order using Eq. (19), (28), and (29), (30) and (32) respectively.
(3) Solve the initial value problem (IVP) ((25)-(27)) to get $u_g,\ u_l$ and ρ_g by a numerical scheme, say RK-(2/4/6) or MSPCM at different steps up to the length of the riser.
(4) Format and print all values of $u_g,\ u_l,\ \rho_g,\ F_D$ and C_D etc.

4 Results and discussion

Analysis has been carried out both with and without cross - sectional variation effects and the obtained results are compared with the experimental values. To begin with the current numerical scheme and the in-house code, validation is carried out in two different ways. Firstly, we compare the approximate solution from different numerical schemes and they are found to be in good agreement. Numerical simulations are carried out for a wide range of governing parameters. As a sample, the results (i.e., ρ_g, u_g, u_l, C_D, F_D, α) obtained by Runge-Kutta Methods of order 2(RK-2), 4(RK-4), 6(RK-6) and those from Milne-Simpson Predictor-Corrector Method (MSPCM) (without accounting for the cross - sectional effects) are provided in Fig. 2where $m_g = 4.7$, $m_l = 43.0$, $p = 6.17778\ kg/sm^2$. From the Fig. 2, it can be easily seen that the approximate solutions obtained from the different methods are in good agreements. Thus, we consider the Runge - Kutta Method of order 4 for further analysis and present the data of approximate solutions obtained from RK-4 (see Tab. 1).

Table 1. Numerical results obtained on using RK-4

X	ρ_g	u_g	u_l	C_D	F_D	α	Flow Regime
0.0000	6.9347	1.4969	0.7484	2.1343	0.2065	0.0954	Distorted Bubble
0.5000	6.2997	0.9889	0.8199	2.3008	0.0121	0.1590	Distorted Bubble
1.0000	5.6708	1.0080	0.8411	2.4076	0.0132	0.1733	Distorted Bubble
1.1000	5.5463	1.0125	0.8461	2.4310	0.0135	0.1764	Distorted Bubble
1.5000	5.0532	1.0329	0.8685	2.5326	0.0146	0.1897	Distorted Bubble
2.0000	4.4489	1.0664	0.9049	2.6809	0.0163	0.2088	Distorted Bubble
2.5000	3.8599	1.1132	0.9548	2.8595	0.0183	0.2305	Distorted Bubble
2.8000	3.5150	1.1508	0.9944	2.9848	0.0198	0.2448	Distorted Bubble
3.0000	3.2907	1.1590	1.0444	1.4616	0.0208	0.2597	Slug - Flow
3.5000	2.7424	1.2775	1.1500	1.3721	0.0245	0.2827	Churn - Turbulent
4.0000	2.2161	1.4598	1.3166	1.2838	0.0302	0.3061	Churn - Turbulent

We also validate our scheme and the in-house computer code by comparing the results obtained from the current numerical simulation based on RK-4 Method for $m_g = 4.7\ kg/s$, $m_l = 43.0\ kg/s$, $p = 6.17778\ kg/sm^2$, $XL = 4.352\ m$, $T = 300.0\ kelvin$, $g = 9.8\ m/s^2$ with the experimental and the computational results reported by Satyamurthy et al.[15]. In Tabs. 2-3 the obtained data related to void fraction and slip based on the current numerical simulation are compared with the results reported by Taitel et al.[17] and Satyamurthy et al.[15]. It is worth noted that the obtained results, both with and without cross-sectional effects, match very well with the experimental data of Taitel et al.[17] and also with the numerical results of Satyamurthy et al.[15].

Table 2. Comparison of void fraction with the experimental and numerical results from literature

$m_g \times 10^3$ $[kg/s]$	m_l $[kg/s]$	α $(expt.)$	Satyamurthy's α	Current α	Satyamurthy's α_{cs}	Current α_{cs}
			At X = 1.1m			
2.5	35.3	0.15	0.11	0.12	0.10	0.10
4.7	43.0	0.20	0.18	0.18	0.16	0.21
7.0	48.8	0.25	0.23	0.23	0.20	0.22
9.0	54.8	0.29	0.27	0.28	0.23	0.22
11.0	58.6	0.32	0.30	0.31	0.26	0.23
			At X = 2.8m			
2.5	35.3	0.18	0.17	0.19	0.15	0.15
4.7	43.0	0.26	0.25	0.27	0.23	0.37
7.0	48.8	0.31	0.31	0.32	0.27	0.32
9.0	54.8	0.36	0.36	0.36	0.31	0.29
11.0	58.6	0.40	0.40	0.40	0.35	0.28

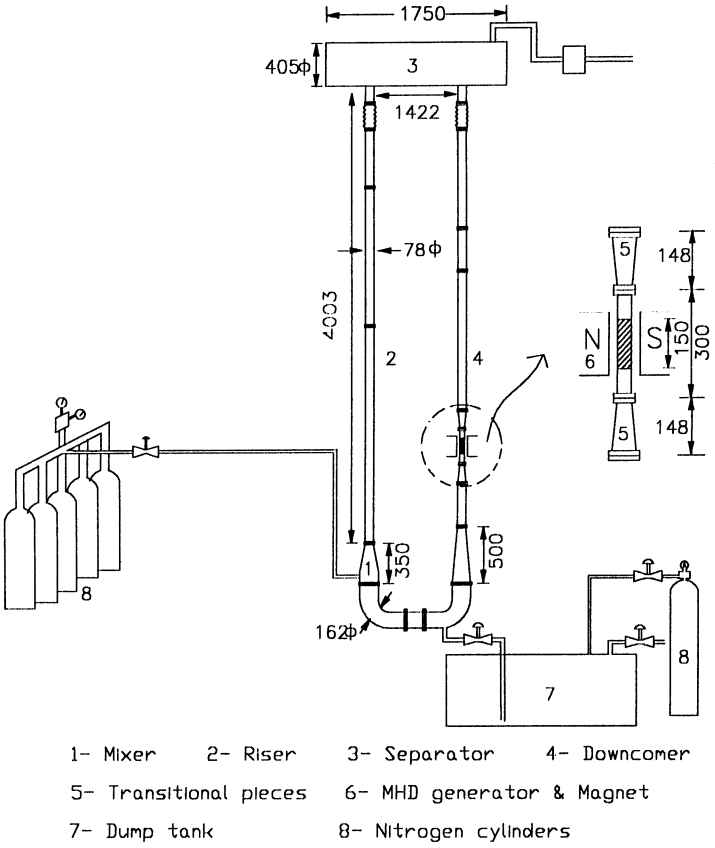

Fig. 1. Schematic of the nitrogenmercury LMMHD experimental facility

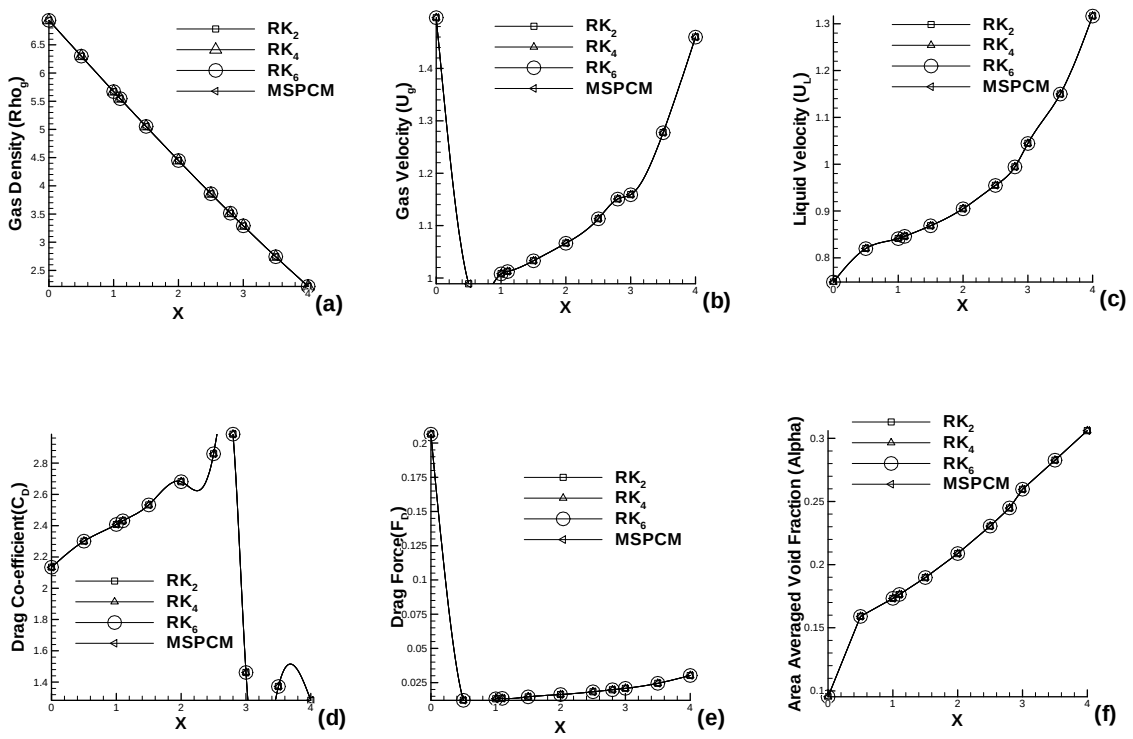

Fig. 2. Comparisons of ρ_g, u_g, u_l, C_D, F_D and α with different methods for the case (m_g, m_l) = (4:7; 43:0)

Table 3. Comparison of slip with the experimental and numerical results from literature

$m_g \times 10^3$ $[kg/s]$	m_l $[kg/s]$	S $(expt.)$	Satyamurthy's S	Current S	Satyamurthy's S_{cs}	Current S_{cs}
			At X = 1.1m			
2.5	35.3	1.2	1.3	1.2	1.5	1.5
4.7	43.0	1.0	1.2	1.2	1.5	1.4
7.0	48.8	1.2	1.2	1.2	1.4	1.4
9.0	54.8	1.1	1.2	1.1	1.4	1.3
11.0	58.6	1.2	1.1	1.1	1.4	1.3
			At X = 2.8m			
2.5	35.3	1.8	1.2	1.2	1.5	1.5
4.7	43.0	1.3	1.2	1.1	1.5	1.4
7.0	48.8	1.5	1.2	1.1	1.5	1.3
9.0	54.8	1.6	1.2	1.1	1.5	1.3
11.0	58.6	1.4	1.1	1.1	1.5	1.3

Influence of mass flow rates of gas phase (m_g) and liquid phase (m_l):

To investigate the influence of m_g and m_l on averaged model, simulations have been carried out for three different sets of $(m_g,\ m_l)$ values, i.e. for $(m_g,\ m_l) = \{(4.7,\ 43.0), (2.5,\ 35.3)$ and $(9.0,\ 54.8)\}$ and we are fixing other parameter as follows: $p = 6.17778\ kg/sm^2$, $XL = 4.352\ m$, $T = 300.0\ kelvin$, $g = 9.8\ m/s^2$. We investigate the flow dynamics both when the mass flow rates are decreased and increased w.r.to those considered for earlier simulation.

The Fig. 2 presents the flow dynamics for the case $(m_g, m_l) = (4.7, 43.0)$. From the Fig. (a) in Fig. 2, one can notice that the density for the gas phase (ρ_g) decreases linearly with the length of the tube. Also, the Fig. b in Fig. 2 shows that the velocity of the gas phase (u_g) initially decreases as one moves along the length of the tube i.e., for $0 \leq\ X\ \leq\ 0.5$ and when $0.5\ \leq\ X\ \leq\ 3.0$, there is a slow raise in u_g. And later for $3.0\ \leq\ X\ \leq\ 4.0$ there is relatively a larger increase in u_g. Further, velocity of the liquid phase (u_l) is seen to gradually increase as one moves along the length of the tube (see Fig. c in Fig. 2). It is also noted that, the extent of the increase in u_l is relatively larger for $3.0\ \leq\ X\ \leq\ 4.0$, i.e., towards the end of the tube. In Fig. d in Fig. 2, the Drag-Coefficient (C_D) is seen to be increasing for $0\ \leq\ X\ <\ 3.0$, however, at $X = 3.0$, a significant fall in C_D is being noticed due to the change in flow regime. In particular, here the flow regime is changing from distorted bubble to churn - turbulent flow regime. Also, for the case $3.0\ \leq\ X\ \leq\ 4.0$, C_D is found to be nearly constant. Moreover, the Drag Force (F_D) is seen to initially undergo a drastic fall but later, for $0.5\ \leq\ X\ \leq\ 4.0$, there is relatively a little raise in F_D (see Fig. e in Fig. 2).

Now, for the case with $m_g = 2.5,\ m_l = 35.3$ and $p = 6.17778\ kg/sm^2$ the results are presented in Tab. 4. From the data in the Tab. 4 one can see that the void fraction (α) increases along the length of the tube. Moreover, the void fraction values indicate that the flow is in Distorted Bubble Regime up to $X = 3.5$ and then at $X = 4.0$ it gets into Churn-Turbulent Flow Regime. Initially there is a fall in velocity of gas phase (u_g) and then it is increasing along the length of the riser. And at $X = 4.0$ there is relatively a big raise in u_g. The velocity of liquid phase (u_l) is gradually increasing along the length of the tube. And at $X = 4.0$ there is relatively a big raise in u_l. The Density (ρ_g) of the gas phase is decreasing as one moves along the length of the riser. Initially there is a big fall in F_D. Then there is a little raise in F_D up to $X = 3.5$. At $X = 4.0,\ F_D$ is seen to undergo a small fall. The drag coefficient (C_D) is increasing along the length of the tube, but a big fall is noticed in C_D at the end of the tube because of change in flow regime. Here the flow regime is seen to change from $X = 3.5$ to $X = 4.0$.

In Tab. 5, we consider the case when $m_g\ =\ 9.0\ kg/s,\ m_l\ =\ 54.8\ kg/s$ and $p\ =\ 6.17778\ kg/sm^2$. Here we see that initially there is a large increment in the void fraction (α) and later it is gradually increasing along the length of the tube. The variation in magnitude of the void fraction values along the length of the tube depicts that for $0.0\ \leq\ X\ <\ 1.1$ flow lies in Distorted Bubble Regime and later it gets into Churn-Turbulent Flow Regime. Also, it can be seen that initially there is a fall in u_g and then it is increasing along the length of the riser. There is relatively a big raise in u_g towards the end of the riser. The velocity of the liquid phase (u_l) is increasing all along the length of the tube. Both initially and towards the end of the riser a big raise in

Table 4. Numerical results obtained on using RK-4 when $m_g = 2.5\ kg/s$, $m_l = 35.3\ kg/s$ and $p = 6.17778\ kg/sm^2$

X	ρ_g	u_g	u_l	C_D	F_D	α	Flow Regime
0.0000	6.9347	1.1668	0.5834	2.7177	0.2693	0.0647	Distorted Bubble
0.5000	6.2615	0.7905	0.6138	2.8863	0.0281	0.1058	Distorted Bubble
1.0000	5.5948	0.7987	0.6236	3.0194	0.0311	0.1172	Distorted Bubble
1.1000	5.4625	0.8006	0.6259	3.0488	0.0317	0.1197	Distorted Bubble
1.5000	4.9373	0.8094	0.6364	3.1774	0.0347	0.1310	Distorted Bubble
2.0000	4.2912	0.8240	0.6536	3.3690	0.0392	0.1481	Distorted Bubble
2.5000	3.6593	0.8448	0.6777	3.6070	0.0449	0.1693	Distorted Bubble
2.8000	3.2884	0.8621	0.6973	3.7800	0.0492	0.1846	Distorted Bubble
3.0000	3.0453	0.8765	0.7134	3.9115	0.0524	0.1961	Distorted Bubble
3.5000	2.4542	0.9287	0.7706	4.3146	0.0628	0.2297	Distorted Bubble
4.0000	1.8969	0.9962	0.9038	1.3939	0.0291	0.2770	Churn - Turbulent

u_l is noticed. Density for the gas phase (ρ_g) is decreasing as one moves along the length of the riser. Initially there is a big fall in F_D and then it is nearly constant along the length of the tube up to $X = 3.0$ and then there is a small increment in F_D. The drag coefficient (C_D) is increasing along the length of the tube when $0.0 \leq X < 1.1$, and there is a big fall in C_D at $X = 1.5$ and later it is decreasing along the length of the tube.

Table 5. Numerical results obtained on using RK-4 when $m_g = 9.0\ kg/s$, $m_l = 54.8\ kg/s$ and $p = 6.17778\ kg/sm^2$

X	ρ_g	u_g	u_l	C_D	F_D	α	Flow Regime
0.0000	6.9347	1.9659	0.9829	1.6953	0.1686	0.1382	Distorted Bubble
0.5000	6.3537	1.3141	1.1545	1.8622	0.0052	0.2257	Distorted Bubble
1.0000	5.7701	1.3599	1.2023	1.9455	0.0056	0.2402	Distorted Bubble
1.1000	5.6547	1.3705	1.2133	1.9635	0.0057	0.2432	Distorted Bubble
1.5000	5.2013	1.3864	1.2921	1.4550	0.0061	0.2613	Churn - Turbulent
2.0000	4.6449	1.4735	1.3727	1.4004	0.0068	0.2753	Churn - Turbulent
2.5000	4.1005	1.5871	1.4790	1.3459	0.0076	0.2896	Churn - Turbulent
2.8000	3.7802	1.6728	1.5598	1.3141	0.0082	0.2980	Churn - Turbulent
3.0000	3.5697	1.7394	1.6230	1.2937	0.0087	0.3035	Churn - Turbulent
3.5000	3.0547	1.9500	1.8240	1.2463	0.0104	0.3164	Churn - Turbulent
4.0000	2.5599	2.2496	2.1120	1.2070	0.0129	0.3272	Churn - Turbulent

From Tabs. 4 and 5, one can see that when one marches along the length of the riser with $(m_g,\ m_l,\ p) = (4.7\ kg/s,\ 43.0\ kg/s,\ 6.17778\ kg/sm^2)$, while the void fraction (α) increases by a factor of 3.21, the density of gas phase (ρ_g) decreases by a factor of 0.68. While u_g initially decreases by a factor of 0.7 and later increases by a factor of 1.48, u_l is seen to increase by a factor of 1.75. C_D gradually increases up to $X = 2.8$ and at $X = 3.0$ it undergoes a sudden fall in its magnitude. Initially F_D decreases by a factor of 0.06 and later it increases by a factor of 2.5. Decreasing $(m_g,\ m_l)$ by a factor of 0.5 leads to a 4.28 factor raise in the variation of void fraction (α) across the length of the riser and 1.6 factor raise in the drag coefficient (C_D) up to the $X = 3.5$ with a sudden fall in its magnitude by a factor of 0.32 at $X = 4.0$. It also leads to a 0.1 factor fall in F_D initially and later a 2.23 factor raise in F_D when $0.5 \leq X \leq 3.5$ and finally a 0.5 factor fall in F_D is noticed at $X = 4.0$. With decreasing mass flow rates while u_l is enhanced by a factor of 1.55, u_g is seen to initially fall by a factor of 0.67 and later is raised by a factor of 1.26. And further, increasing $(m_g,\ m_l)$ by a factor of 0.5 leads to a raise in void fraction (α) by a factor of 2.37 and a 1.2 factor raise in the variation of drag coefficient (C_D) up to $X = 1.1$ with a sudden fall in its magnitude at $X = 1.5$ by a factor of 0.74 and later it decreases by a factor of 0.8. Increasing $(m_g,\ m_l)$ by a factor of 0.5 leads to a 0.03 factor fall in F_D initially and later a 2.5 factor raise along the length of the riser. With increasing mass flow rates while u_l is enhanced by a factor of 2.15, u_g is seen to initially fall by a factor of 0.60 and later is raised by a factor of 1.70.

Influence of pressure:

Next, we investigate the influence of variation of pressure (p) on the combined two phase momentum flow model. We investigate the flow dynamics both when the pressure is decreased and increased w.r.t those considered for earlier simulation. For the case with $m_g = 4.7,\ m_l = 43.0$ and $p = 3.08889\ kg/sm^2$ the results are presented in Tab. 6. From the data in the Tab. 6 one can see that the void fraction (α) is increasing along the length of the tube. It is noticed that initially the flow lies in Distorted Bubble Regime but afterwards (i.e. for $X > 0.5$) flow lies in Churn-Turbulent Flow regime. Also, initially there is a fall in u_g and then it is increasing along the length of the riser. As one moves from $X = 0.5$ to $X = 1.5$ there is relatively little raise in u_g but when one moves away from $X = 2.0$ there is relatively a large raise in u_g along the remaining length of the tube. One can also see from the Tab. 7 that there is a little raise in u_l from $X = 0.0$ to $X = 2.0$, whereas from $X = 2.0$ to $X = 4.0$ a significant raise in u_l is noticed. Density for the gas phase (ρ_g) is decreasing as one moves along the length of the riser. Initially there is a big fall in F_D and then a small raise up to $X = 3.0$ is noticed. Further up there is small increment in F_D. C_D undergoes a big fall at $X = 0.5$ and then it is decreasing gradually along the length of the riser up to $X = 3.0$. Later a small increment in C_D is noticed.

Table 6. Numerical results obtained on using RK-4 when $m_g = 4.7\ kg/s$ and $m_l = 43.0\ kg/s$ with pressure $p = 3.08889\ kg/sm^2$

X	ρ_g	u_g	u_l	C_D	F_D	α	Flow Regime
0.0000	3.4673	1.6397	0.8198	2.2531	0.2616	0.1742	Distorted Bubble
0.5000	2.9330	1.1956	1.0835	1.3731	0.0114	0.2824	Churn - Turbulent
1.0000	2.4039	1.3541	1.2292	1.2908	0.0138	0.3043	Churn - Turbulent
1.1000	2.3007	1.3954	1.2676	1.2752	0.0144	0.3085	Churn - Turbulent
1.5000	1.8989	1.6091	1.4686	1.2182	0.0178	0.3241	Churn - Turbulent
2.0000	1.4291	2.0463	1.8850	1.1663	0.0256	0.3387	Churn - Turbulent
2.5000	1.0229	2.8004	2.6085	1.1415	0.0434	0.3457	Churn - Turbulent
2.8000	0.8296	3.4404	3.2250	1.1371	0.0624	0.3470	Churn - Turbulent
3.0000	0.7262	3.9291	3.6979	1.1366	0.0787	0.3471	Churn - Turbulent
3.5000	0.5460	5.2364	4.9720	1.1393	0.1258	0.3464	Churn - Turbulent
4.0000	0.4405	6.5112	6.2244	1.1431	0.1728	0.3453	Churn - Turbulent

Now, for the case with $m_g = 4.7\ kg/s,\ m_l = 43.0\ kg/s$ and $p = 9.26667\ kg/sm^2$ the results are presented in Tab. 7. From the data in the Tab. 7 one can see that the void fraction (α) is increasing along the length of the riser. From the magnitudes of the void fraction, it can be inferred that the flow in the entire length of the riser lies just in Distorted Bubble Regime only. Initially there is a fall in u_g and then there is relatively little raise along the length of the tube. Also, there is relatively a small raise in both u_l and C_D as when one moves along the length of the tube. Density of the gas phase (ρ_g) is decreasing along the length of the tube. Initially there is a fall in F_D and then it is seen to raise as one moves along the length of the tube.

Table 7. Numerical results obtained on using RK-4 when $m_g = 4.7\ kg/s$ and $m_l = 43.0\ kg/s$ with pressure $p = 9.26667\ kg/sm^2$

X	ρ_g	u_g	u_l	C_D	F_D	α	Flow Regime
0.0000	10.4020	1.4493	0.7246	2.0944	0.1900	0.0657	Distorted Bubble
0.5000	9.7305	0.9406	0.7640	2.2004	0.0124	0.1082	Distorted Bubble
1.0000	9.0618	0.9474	0.7718	2.2640	0.0132	0.1154	Distorted Bubble
1.1000	8.9287	0.9488	0.7735	2.2775	0.0134	0.1169	Distorted Bubble
1.5000	8.3987	0.9553	0.7809	2.3347	0.0141	0.1234	Distorted Bubble
2.0000	7.7419	0.9648	0.7918	2.4139	0.0152	0.1326	Distorted Bubble
2.5000	7.0922	0.9763	0.8049	2.5035	0.0164	0.1430	Distorted Bubble
2.8000	6.7062	0.9845	0.8141	2.5631	0.0172	0.1500	Distorted Bubble
3.0000	6.4507	0.9906	0.8210	2.6057	0.0178	0.1550	Distorted Bubble
3.5000	5.8186	1.0086	0.8411	2.7235	0.0195	0.1688	Distorted Bubble
4.0000	5.1975	1.0320	0.8668	2.8611	0.0214	0.1847	Distorted Bubble

From Tabs. 6 and 7, one can see that decreasing pressure by a factor of 0.5 leads to a fall in the variation of the void fraction (α) across the length of the riser by a factor of 1.23 and in the variation of density of gas phase (ρ_g) by a factor of 0.13, whereas increasing the pressure by a factor of 0.5 leads to a fall in the variation of the void fraction (α) by a factor of 0.4 and in the variation of ρ_g by a factor of 0.5. While decreasing pressure by a factor of 0.5 leads a 0.5 factor fall in C_D and a 0.04 factor fall in F_D initially and later a raises it by a factor of 15.14, increasing pressure by a factor of 0.5 leads a raise in C_D by a factor of 1.4 and an initial fall in F_D by a factor of 0.07 with a 0.2 factor raise towards the end of the riser.

5 Summary and conclusions

An averaged two-fluid model for dispersed vertical two-phase flow of Bubbles, Drops and Particles consisting of one-dimensional combined momentum equation, bubble momentum equation and continuity equations for gas and liquid phase along with the auxiliary equations has been analyzed. The two phase fluid flow is found to be highly sensitive both to the magnitudes of liquid and gas mass flow rates i.e., $(m_g,\ m_l)$ and also to the inlet pressure (p).

While the gas and liquid velocities $(u_g,\ u_l)$ together with area averaged void fraction for gas phase (α) are increasing with increasing mass flow rates the drag co-efficient for multiple species and drag force (C_D and F_D) are found to be decreasing. Increasing mass flow rates enhance the variation of density of gas phase (ρ_g) by nearly 10% across the length of the riser. It is being noticed that flow behaves differently at different locations of the riser at all the mass flow rates. Both distorted-bubble and churn - turbulent flows are being noticed in the riser. The flow which is noticed to be largely in distorted-bubble regime at smaller mass flow rates depicts churn-turbulent flow nature with increasing mass flow rates. With increasing pressure while $u_g,\ u_l,\ C_D,\ F_D$ and α are decreasing ρ_g is found to be increasing. At small pressures the flow lies largely in churn-turbulent regime. On increasing the pressure, at different spatial regions of the riser, flow behaves differently. Initially it is a distorted bubble flow and later depicts slug flow behavior before finally ending up as a churn-turbulent flow. On further increasing the pressure, flow completely gets into distorted bubble regime.

Appendix

Nomenclature

A	Cross - sectional area of the pipe (m^2)
A_d	Projected area of the bubble (m^2)
a_i	Interfacial area per unit volume (m^2/m^3)
B_d	Volume of a typicalparticle
C_D	Drag Coefficient for multi - particles system
C_{D_∞}	Drag Coefficient for a single particle system
C_{vm}	Virtual mass coefficient (dimensionless)
D	Diameter of the pipe (m)
f_{lo}	Friction coefficient for liquid metal only
f_{go}	Friction coefficient for gas metal only
f_R	Friction factor
fr_{lo}	Friction with liquid only
F_r	Froude number (dimensionless)
F_D	Drag force (N)
F_{vm}	Virtual Mass Force (N)

g	Acceleration due to gravity (m/s^2)
I_E	Entrance length for Transition to Slug flow(m)
m_k	Mass flow rates (kg/s) for k - phase
M_{id}	Generalized interfacial drag force acting on dispersed phase
M_{ik}	Generalized interfacial drag force of k-phase
N_{Re_∞}	Single Particle Reynolds number
N_{Re}	Particle Reynolds number
N'_{Re}	The Reynolds number of flow in the pipe
p	Pressure
r_d	Particle radius
r_d^o	Non -dimensional radius
R	The gas constant
t	Time
T	Temperature
u_k	Averaged mean velocity for k-phase (See Ishii, M., 1984[9])
v_k	Velocity of k - phase
v_r	Relative velocity $(v_d - v_c)$
v_{r_∞}	Terminal velocity for a single particle system
$v_{r_\infty}^o$	Non - dimensional velocity
V_b	Volume of the bubble (m^3)
W_e	Weber number (dimensionless)
Q	Quality (dimensionless)
XL	Length of the tube
X	Axial coordinate

Greek symbols

α	Area Averaged Void fraction for gas phase
α_k	Area Averaged Void fraction of k-phase (See Ishii, M., 1984[9])
α_{dm}	Maximum packing void fraction
Γ_k	Masssource for k - phase
$\triangle\rho$	Absolute value of density difference
μ_k	Viscosity of k-phase
μ_m	Mixture viscosity in dispersed flow
ρ_k	Density of k - phase
ρ_m	Density of mixture
σ	Interfacial Tension
$\bar{\bar{\tau}}_k$	Averaged viscous stress for k-phase
$\bar{\bar{\tau}}_k^T$	Turbulent stress for k-phase
φ_{lo}^2	Two - Phase multiplier for liquid metal only
ϵ	The internal surface roughness factor of the pipe

Subscripts

c	Continuous phase
cs	Cross-sectional variations accounted
d	Dispersed phase
l	Liquid phase
g	Gas or Vapor phase
k	k - phase ($k = c, d$ or $k = g, l$)
ki	k - phase at interface
m	Mixture

References

[1] M. L. de Bertodano, W. Fullmer, A. Vaidheeswaran. One-dimensional two-equation two-fluid model stability. *Multiphase Science and Technology*, 2013, **25**(2–4).

[2] F. Friedel. Improved friction pressure drop correlations for horizontal and vertical two-phase pipe flow. **in:** *European two-phase flow group meeting, Paper E*, vol. 2, 1979.

[3] W. Fullmer, A. Clausse, et al. Numerical solution of wavy-stratified fluid-fluid flow with the one-dimensional two-fluid model: Stability, boundedness, convergence and chaos. **in:** *ASME 2014 4th Joint US-European Fluids Engineering Division Summer Meeting collocated with the ASME 2014 12th International Conference on Nanochannels, Microchannels, and Minichannels*, American Society of Mechanical Engineers, 2014, V002T20A006–V002T20A006.

[4] R. Giles. Fluid mechanics and hydraulics. *Schaum's outline series*, 1983, McGraw - Hill, Singapore.

[5] H. Guo, Z. Guo. Existence and uniqueness of global strong solutions to a free boundary value problem for a one-dimensional viscous two-phase model. *Acta Mathematicae Applicatae Sinica*, 2013, **36**: 62–81.

[6] W. D. Fullmer, M. A. Lopez de Bertodano, X. Zhang. Verification of a higher-order finite difference scheme for the one-dimensional two-fluid model. *The Journal of Computational Multiphase Flows*, 2013, **5**(2): 139–156.

[7] M. Ishii. One-dimensional drift-flux model and constitutive equations for relative motion between phases in various two-phase flow regimes. *Tech. Rep.*, Argonne National Lab., Ill.(USA), 1977.

[8] M. Ishii, T. Hibiki. *Thermo-fluid dynamics of two-phase flow*. Springer Science & Business Media, 2010.

[9] M. Ishii, K. Mishima. Two-fluid model and hydrodynamic constitutive relations. *Nuclear Engineering and design*, 1984, **82**(2): 107–126.

[10] M. Ishii, N. Zuber. Drag coefficient and relative velocity in bubbly, droplet or particulate flows. *AIChE Journal*, 1979, **25**(5): 843–855.

[11] A. Kumar, T. Degaleesan, et al. Bubble swarm characteristics in bubble columns. *The Canadian Journal of Chemical Engineering*, 1976, **54**(6): 503–508.

[12] H. Luther. An explicit sixth-order runge-kutta formula. *Mathematics of Computation*, 1968, 434–436.

[13] P. Varadarajan, P. Hammond. Numerical scheme for accurately capturing gas migration described by 1D multiphase drift flux model. *International Journal of Multiphase Flow*, 2015, **73**: 57–70.

[14] R. Roscoe. The viscosity of suspensions of rigid spheres. *British Journal of Applied Physics*, 1952, **3**(8): 267.

[15] P. Satyamurthy, N. Dixit, T. Thiyagarajan, N. Venkatramani, A. Quraishi, A. Mushtaq. Two-fluid model studies for high density two-phase liquid metal vertical flows. *International journal of multiphase flow*, 1998, **24**(5): 721–737.

[16] J. Solsvik, Z. Chao, H. Jakobsen. Numerical evaluation of a one-dimensional two-fluid model applied to gas–solid cold-flows in fluidised beds. *The Canadian Journal of Chemical Engineering*, 2014, **92**(3): 401–420.

[17] Y. Taitel, D. Bornea, A. Dukler. Modelling flow pattern transitions for steady upward gas-liquid flow in vertical tubes. *AIChE Journal*, 1980, **26**(3): 345–354.

[18] G. Taylor. The viscosity of a fluid containing small drops of another fluid. *Proceedings of the Royal Society of London. Series A, Containing Papers of a Mathematical and Physical Character*, 1932, 41–48.

[19] T. Thiyagarajan, P. Satyamurthy, et al. Void fraction profile measurements in two-phase mercuryłnitrogen flows using gamma-ray attenuation method. *Experimental thermal and fluid science*, 1995, **10**(3): 347–354.

[20] N. Zuber. On the dispersed two-phase flow in the laminar flow regime. *Chemical Engineering Science*, 1964, **19**(11): 897–917.